

# Heterogeneously Catalyzed Thioether Metathesis by a Supported Au–Pd Alloy Nanoparticle Design Based on Pd Ensemble Control

Takehiro Matsuyama<sup>†</sup>, Takafumi Yatabe<sup>\*,†,‡</sup>, Tomohiro Yabe<sup>†</sup>, Kazuya Yamaguchi<sup>\*,†</sup>

<sup>†</sup>Department of Applied Chemistry, School of Engineering, The University of Tokyo, 7-3-1 Hongo, Bunkyo-ku, Tokyo 113-8656, Japan.

<sup>‡</sup>Precursory Research for Embryonic Science and Technology (PRESTO), Japan Science and Technology Agency (JST), 4-1-8 Honcho, Kawaguchi, Saitama 332-0012, Japan.

\*e-mail: kyama@appchem.t.u-tokyo.ac.jp, yatabe@appchem.t.u-tokyo.ac.jp.

KEYWORDS: Au–Pd alloy nanoparticle, metathesis, thioethers, ensemble effect, heterogeneous catalysis

**ABSTRACT:** C–S bond metathesis of thioethers has gained attention as a new approach to the late-stage diversification of already existing useful thioethers with intact molecular frameworks. However, direct or indirect thioether metathesis is scarcely reported, and heterogeneously catalyzed systems have not been explored. Here, we develop heterogeneously catalyzed direct thioether metathesis using a supported Au–Pd alloy nanoparticle catalyst with a high Au/Pd ratio. The Au-diluted Pd ensembles suppress the strong  $\pi$ -adsorption of diaryl thioethers on the nanoparticles and promote transmetalation via thiolate spill-over onto neighboring Au species, enabling an efficient direct thioether metathesis.

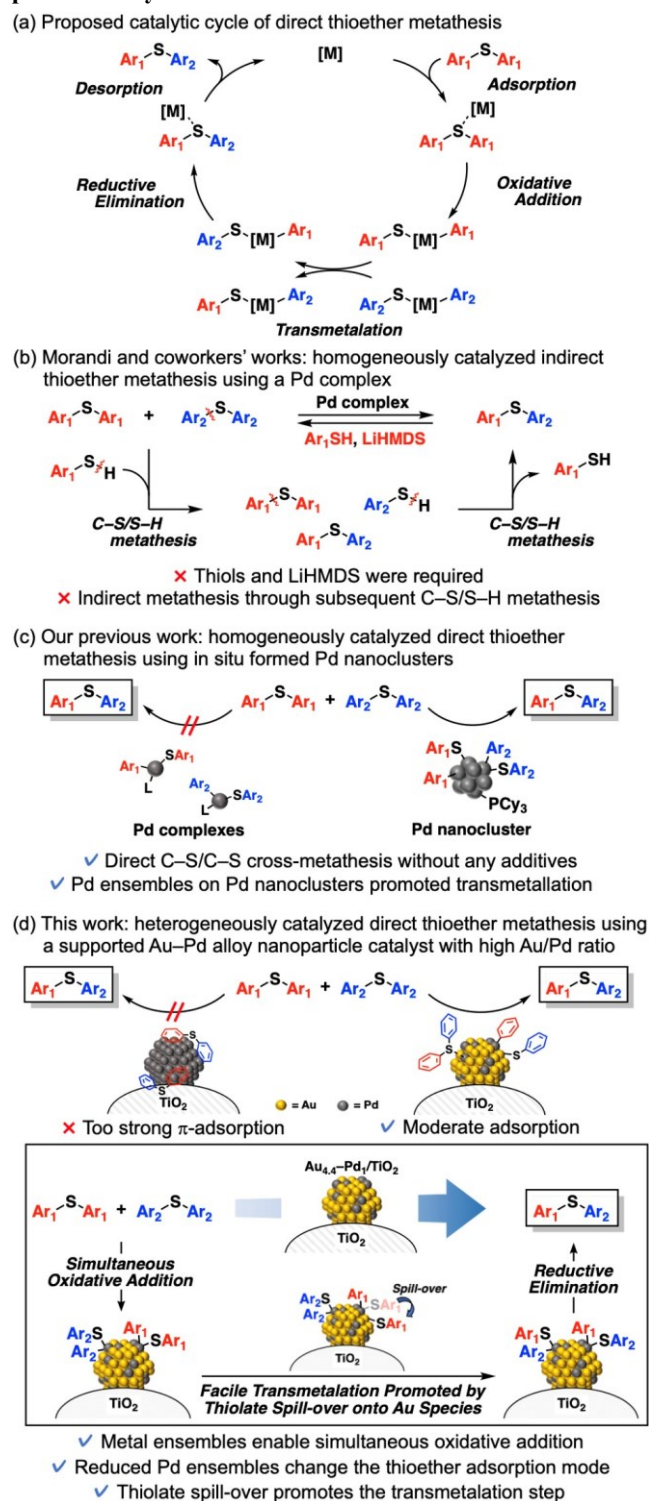
Multimetallic nanocatalysts can exhibit higher catalytic performance and/or selectivity than their monometallic counterparts. This high performance is usually attributed to three alloy effects—ensemble, ligand, and strain effects<sup>1</sup>—which are difficult to study in isolation. Nevertheless, according to some reports, the dominant effect is metal ensembles on the nanoparticle surfaces.<sup>1a</sup> The decreased ensembles of active metal species alter the adsorption configuration of molecules<sup>2</sup> or exhibit a single atom-like character,<sup>3</sup> resulting in unique catalytic properties. Such catalyst designs based on ensemble control are uniquely applicable to nanoparticle catalysts and have the potential to realize novel molecular transformations.

Diaryl thioethers are widely used in polymers, natural products, bioactive compounds, and pharmaceuticals.<sup>4a–c</sup> Late-stage diversification of diaryl thioethers, which enables functionalization and transformation of complex molecules without disrupting their building blocks, has therefore become an important goal in synthetic organic chemistry, medicinal science, and materials science.<sup>4</sup> One desirable approach is C–S bond metathesis of diaryl thioethers, which synthesizes novel diaryl thioethers from already existing useful thioethers. The first C–S bond metathesis of diaryl thioethers was reported by Morandi *et al.*,<sup>5a</sup> who also constructed porous organic polymers with two- and three-dimensional cores under mild reaction conditions (~80°C) using a homogeneous Pd complex catalyst.<sup>5b</sup> Theoretically, direct C–S bond metathesis of diaryl thioethers can proceed through the following catalytic cycle: adsorption and oxidative addition of thioethers to Pd species, transmetalation between oxidative adducts, and then reductive elimination and desorption of thioethers from Pd species (Scheme 1a). However, the direct metathesis does not occur in their reports possibly because the transmetalation step is

prohibitively difficult on Pd complex catalysts. Thus, thiols and lithium bis(trimethylsilyl)amide are required for their reaction systems: indirect C–S/C–S cross-metathesis via C–S/S–H metathesis between diaryl thioethers and thiols (Scheme 1b).<sup>6</sup> Recently, we achieved a direct C–S bond metathesis of diaryl thioethers using only Pd acetate and tricyclohexylphosphine (PCy<sub>3</sub>) as catalyst precursors.<sup>7</sup> The active species of metathesis was confirmed as *in situ*-formed Pd nanoclusters, which likely enable direct crossover between two oxidative adducts (Scheme 1c). However, heterogeneously catalyzed C–S bond metathesis of diaryl thioethers, including indirect metathesis, is demanded for practical use and green sustainable chemistry but has not been attained. In fact, supported monometallic Pd nanoparticles hardly catalyze C–S bond metathesis between phenyl sulfide (**1a**) and *p*-tolyl sulfide (**1b**), even with PCy<sub>3</sub> (Table S1).<sup>7</sup> Clearly, an additional catalyst design is required for heterogeneously catalyzed thioether metathesis.

This study proposes a heterogeneously catalyzed efficient direct C–S bond metathesis of diaryl thioethers using a TiO<sub>2</sub>-supported Au–Pd alloy nanoparticle catalyst (Au<sub>4.4</sub>–Pd<sub>1</sub>/TiO<sub>2</sub>) without any additives (Scheme 1d). This catalytic system exhibits a wide substrate scope and functional group tolerance; moreover, the catalyst can be reused several times. Catalyst characterization and density functional theory (DFT) calculations of cluster models showed that when the Pd ensembles are diluted by Au alloying, the changed adsorption mode of thioethers on the nanoparticles lowers the adsorption/desorption energy and enables C–S bond metathesis. We also suggest that oxidative addition of thioethers produces thiolate species on the Pd species, which migrate to the Au species and promote the transmetalation step, thereby achieving efficient thioether metathesis.

## Scheme 1. Background (a)–(c) and (d) overview of the present study.



Au<sub>4.4</sub>-Pd<sub>1</sub>/TiO<sub>2</sub> was prepared via simultaneous deposition–precipitation of Au and Pd hydroxides (Au/Pd molar ratio = 4.4) on TiO<sub>2</sub>, followed by reduction using NaBH<sub>4</sub> in deionized water. The Pd K-edge and Au L<sub>III</sub>-edge X-ray absorption near edge structure (XANES) spectra of Au<sub>4.4</sub>-Pd<sub>1</sub>/TiO<sub>2</sub> were similar to those of Pd foil and Au foil, respectively (Figure 1a, b), indicating zero valence of Pd and Au, as inferred from the Pd 3d and Au 4f X-ray photoelectron spectra of Au<sub>4.4</sub>-Pd<sub>1</sub>/TiO<sub>2</sub>

(Figure S1). From high-angle annular dark-field–scanning transmission electron microscopy (HAADF–STEM) images, the mean diameter of the TiO<sub>2</sub>-supported metal nanoparticles was determined as 3.05 nm ( $\sigma = 0.77$  nm; Figure 1c, d). From the almost coincident locations of Pd and Au species in the STEM–energy-dispersive spectroscopy (EDS) mapping of Au<sub>4.4</sub>-Pd<sub>1</sub>/TiO<sub>2</sub> (Figure 1e–g) and the fitting of the Pd K-edge and Au L<sub>III</sub>-edge extended X-ray absorption fine structure spectra (indicating that the scatterings originated from Au–Pd

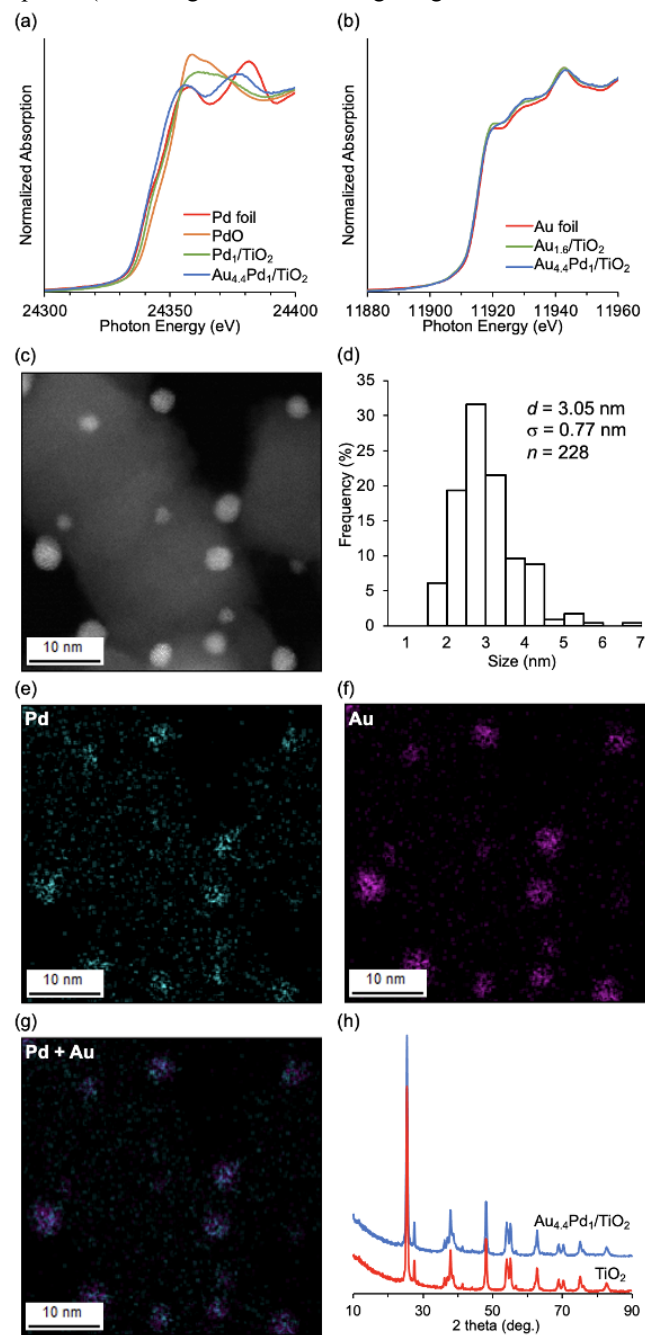


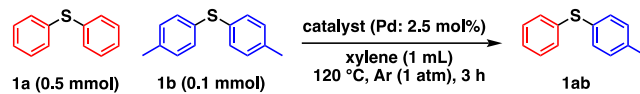
**Figure 1.** Characterization of Au<sub>4.4</sub>-Pd<sub>1</sub>/TiO<sub>2</sub>: (a) Pd K-edge and (b) Au L<sub>III</sub>-edge XANES spectra and (c) HAADF–STEM image of Au<sub>4.4</sub>-Pd<sub>1</sub>/TiO<sub>2</sub>; (d) size distribution of nanoparticles on Au<sub>4.4</sub>-Pd<sub>1</sub>/TiO<sub>2</sub>; (e)–(g) STEM–EDS mappings of Au<sub>4.4</sub>-Pd<sub>1</sub>/TiO<sub>2</sub> showing the distributions of Pd [cyan, panel (e)] and Au [magenta, panel (f)]; (g) overlap of (e) and (f); (h) XRD patterns of TiO<sub>2</sub> and Au<sub>4.4</sub>-Pd<sub>1</sub>/TiO<sub>2</sub>.

bonds; see Figure S2 and Table S2), we inferred that Au–Pd alloy nanoparticles were supported on TiO<sub>2</sub>. Moreover, the X-ray diffraction (XRD) patterns of Au<sub>4.4</sub>–Pd<sub>1</sub>/TiO<sub>2</sub> and TiO<sub>2</sub> were comparable (Figure 1h), confirming that the TiO<sub>2</sub> structure was unchanged during the catalyst preparation.

Table 1 lists the reaction conditions for investigating the effect of Pd-based supported nanoparticle catalysts on C–S bond metathesis between **1a** and **1b**. A quantitative metathesis can obtain two equivalents of phenyl *p*-tolyl sulfide (**1ab**) on the basis of **1b**. Based on our previous report,<sup>7</sup> we first investigated a monometallic TiO<sub>2</sub>-supported Pd nanoparticle catalyst but **1ab** was hardly obtained (Table 1, entry 1).<sup>8</sup> Among several TiO<sub>2</sub>-supported Pd-based bimetallic nanoparticle catalysts, the Au–Pd alloy nanoparticle catalyst exhibited the highest catalytic performance for C–S bond metathesis (Table S3). We therefore prepared supported Au–Pd alloy nanoparticle catalysts with various Au/Pd ratios (Au<sub>x</sub>–Pd<sub>1</sub>/TiO<sub>2</sub>, *x*: Au/Pd molar ratio). The catalytic performance of metathesis improved with increasing Au/Pd ratio in the catalyst, reaching a **1ab** yield of 55% for Au<sub>4.4</sub>–Pd<sub>1</sub>/TiO<sub>2</sub> (Table 1, entries 2–5). Au<sub>1.6</sub>/TiO<sub>2</sub> hardly catalyzed the reaction and a physical mixture of Au<sub>1.6</sub>/TiO<sub>2</sub> and Pd<sub>1</sub>/TiO<sub>2</sub> did not improve the **1ab** yield (Table 1, entries 6 and 7), indicating that Au–Pd alloy formation is essential for the present C–S bond metathesis. After optimizing the supports (Table S4), solvents (Table S5), reaction temperatures (Table S6), and **1a/1b** ratio (Table S7), **1ab** was efficiently produced in 77% yield (Table 1, entry 8). Au<sub>4.4</sub>–Pd<sub>1</sub>/TiO<sub>2</sub> was confirmed to function as the heterogenous catalyst by a hot filtration test and inductively coupled plasma–atomic emission spectroscopy (ICP–AES) (Figure S3), and the catalyst could be reused several times (Figure S4).<sup>9</sup>

Scheme 2a summarizes the substrate scope of Au<sub>4.4</sub>–Pd<sub>1</sub>/TiO<sub>2</sub>-catalyzed C–S bond metathesis of diaryl thioethers. Symmetrical methyl-substituted thioethers at the *para*, *meta*, and *ortho* positions afforded the corresponding unsymmetrical thioethers in good yields (**1ab–1ad**). Other electron-donating groups, including 4-*tert*-butyl and 4-methoxy groups, also afforded their metathesis products (**1be**, **1af**). This system is applicable to thioether metathesis with electron-withdrawing trifluoromethyl groups (**1ag**, **1ah**) and halogenated thioethers with fluoro and chloro groups (**1bi**, **1bj**). 4-Biphenyl-, 2-naphthyl-, and 4-pyridyl-substituted thioethers also served as competent metathesis partners (**1bk**, **1bl**, **1am**). Thioethers with amino (**1an**), *N,N*-dimethylamino (**1bo**), cyano (**1bp**), nitro (**1aq**), acetamide (**1br**), methyl ester (**1bs**), and acetyl (**1bt**) functional groups were converted into the corresponding unsymmetrical thioethers without disrupting the functional groups. Moreover, commercial polyphenylene sulfide (PPS, **1a'**) decomposed into 1,4-bis[(4-methylphenyl)thio]benzene (**1bab**) via metathesis between **1a'** and **1b** in the presence of Au<sub>4.4</sub>–Pd<sub>1</sub>/TiO<sub>2</sub> (Scheme 2b). Gram-scale synthesis from **1a** and **1f** afforded the metathesis product **1af** (1.10 g, 63% isolated yield) (Scheme 2c).

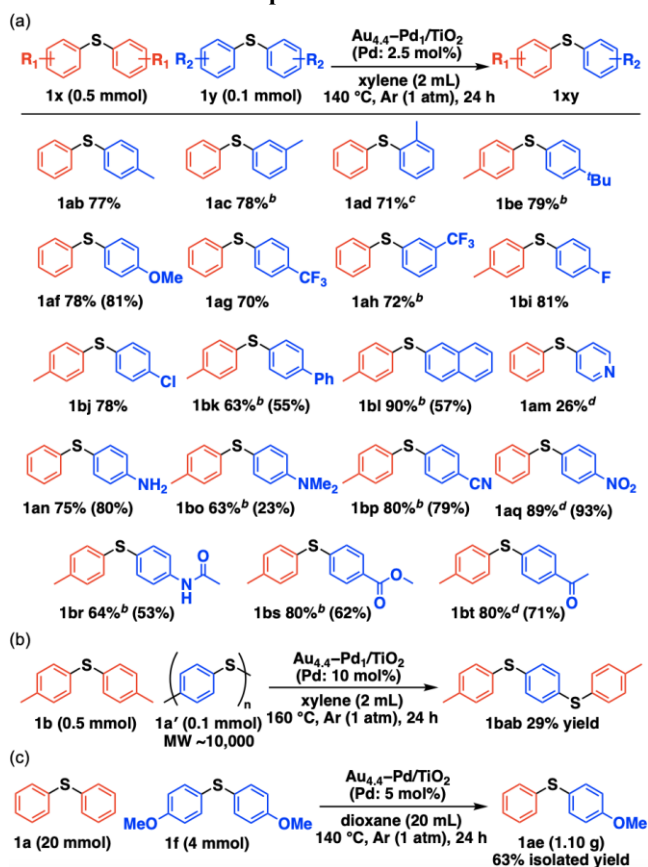
**Table 1.** Effect of catalysts on the metathesis of **1a** and **1b**.<sup>a</sup>



entry	catalyst	Conversion (%)		Yield (%)
		<b>1a</b>	<b>1b</b>	<b>1ab</b>
1	Pd <sub>1</sub> /TiO <sub>2</sub>	9	11	1
2	Au <sub>0.7</sub> –Pd <sub>1</sub> /TiO <sub>2</sub>	9	20	11
3	Au <sub>1.4</sub> –Pd <sub>1</sub> /TiO <sub>2</sub>	14	36	25
4	Au <sub>3.0</sub> –Pd <sub>1</sub> /TiO <sub>2</sub>	19	62	52
5	Au <sub>4.4</sub> –Pd <sub>1</sub> /TiO <sub>2</sub>	18	66	55
6 <sup>b</sup>	Au <sub>1.6</sub> /TiO <sub>2</sub>	10	8	<1
7 <sup>b</sup>	Pd <sub>1</sub> /TiO <sub>2</sub> + Au <sub>1.6</sub> /TiO <sub>2</sub>	<1	3	3
8 <sup>c</sup>	Au <sub>4.4</sub> –Pd <sub>1</sub> /TiO <sub>2</sub>	21	84	77

<sup>a</sup>Conditions: **1a** (0.5 mmol), **1b** (0.1 mmol), catalyst (Pd: 2.5 mol%), xylene (2 mL), 120°C, 3 h, Ar (1 atm). Conversions and yields were determined by GC. <sup>b</sup>Au<sub>1.6</sub>/TiO<sub>2</sub> (Au: 4.0 mol%). <sup>c</sup>140°C, 24 h.

**Scheme 2.** Substrate scope.<sup>a</sup>



(a) Diaryl thioether metathesis. <sup>a</sup>Conditions: **1x** (0.5 mmol), **1y** (0.1 mmol), Au<sub>4.4</sub>–Pd<sub>1</sub>/TiO<sub>2</sub> (Pd: 2.5 mol%), xylene (2 mL), 140°C, 24 h, Ar (1 atm). Yields were determined by GC. Values in parentheses are isolated yields. <sup>b</sup>Au<sub>4.4</sub>–Pd<sub>1</sub>/TiO<sub>2</sub> (Pd: 5 mol%). <sup>c</sup>Au<sub>4.4</sub>–Pd<sub>1</sub>/TiO<sub>2</sub> (Pd: 10 mol%). <sup>d</sup>Au<sub>2.6</sub>–Pd<sub>1</sub>/HAP (Pd: 10 mol%). (b) Polymer decomposition via thioether metathesis. Conditions are indicated in the scheme. The GC yield is shown. (c) Large-scale thioether metathesis. Conditions are indicated in the scheme.



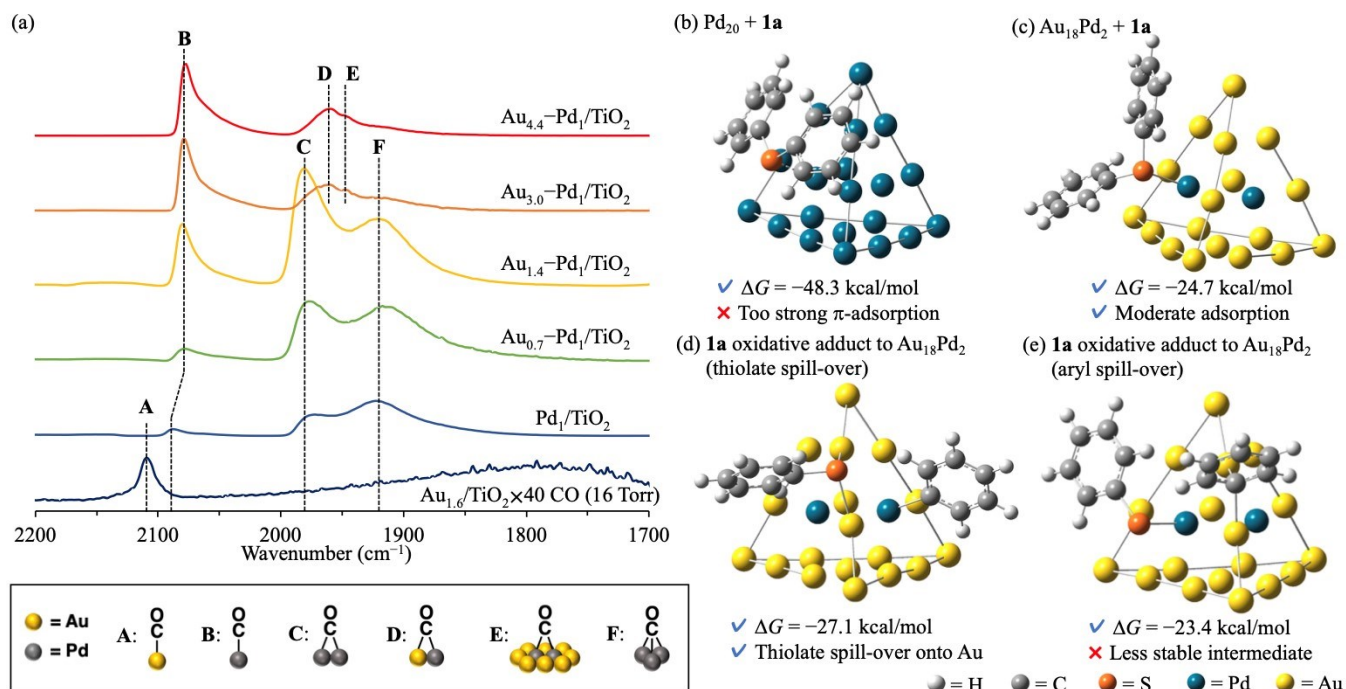


**Figure 2.** Characterization of Au–Pd alloy nanoparticle catalysts and DFT calculations of **1a** adsorption using Pd<sub>20</sub> and Au<sub>18</sub>Pd<sub>2</sub> cluster models: (a) CO–DRIFT spectra of Au<sub>1.6</sub>/TiO<sub>2</sub>, Pd<sub>1</sub>/TiO<sub>2</sub>, and Au<sub>x</sub>-Pd<sub>1</sub>/TiO<sub>2</sub>; optimized structures of **1a** adsorbed on (b) Pd<sub>20</sub> and (c) Au<sub>18</sub>Pd<sub>2</sub>; optimized structures of **1a** oxidative adduct on (d) Au<sub>18</sub>Pd<sub>2</sub> (thiolate spill-over to Au) and (e) Au<sub>18</sub>Pd<sub>2</sub> (aryl spill-over to Au).

The effect of alloying on the present C–S bond metathesis of thioethers was determined from diffuse reflectance infrared Fourier transform (CO–DRIFT) spectra of adsorbed CO on Au<sub>1.6</sub>/TiO<sub>2</sub>, Pd<sub>1</sub>/TiO<sub>2</sub>, and Au<sub>x</sub>-Pd<sub>1</sub>/TiO<sub>2</sub> (Figure 2a). In the CO–DRIFT spectra of Pd<sub>1</sub>/TiO<sub>2</sub>, Au<sub>0.7</sub>-Pd<sub>1</sub>/TiO<sub>2</sub>, and Au<sub>1.4</sub>-Pd<sub>1</sub>/TiO<sub>2</sub>, which exhibited low catalytic activity for the C–S bond metathesis (Table 1, entries 1–3), three peaks around 2070, 1980, and 1920 cm<sup>-1</sup> were observed assignable to linear (**B**), bridged (**C**), and three-fold (**F**) CO species on zero-valent Pd species, respectively.<sup>10</sup> In the CO–DRIFT spectra of Au<sub>3.0</sub>-Pd<sub>1</sub>/TiO<sub>2</sub> and Au<sub>4.4</sub>-Pd<sub>1</sub>/TiO<sub>2</sub> showing high catalytic activity (Table 1, entries 4 and 5), peaks C and F were absent while new peaks at 1950 and 1940 cm<sup>-1</sup> were attributable to CO species bridged on Au and Pd species (**D**) and on Pd species surrounded by Au species (**E**), respectively.<sup>10d</sup> As the Pd and Au–Pd alloy nanoparticles were similarly sized (Figures 1c, d, and S5) and the peak of the CO species on Pd did not shift with increasing Au/Pd ratio in Au<sub>x</sub>-Pd<sub>1</sub>/TiO<sub>2</sub> (Figure 2a), we attributed the high catalytic activity of Au<sub>4.4</sub>-Pd<sub>1</sub>/TiO<sub>2</sub> to the diluted Pd ensembles rather than to the ligand effect.

Next, the ensemble effect on the present C–S bond metathesis was investigated through DFT calculations on Pd<sub>20</sub> and Au<sub>18</sub>Pd<sub>2</sub> cluster models. Referring to previous reports, we adopted Gaussian 16 (M06 functional with SDD basis sets for Au and Pd and 6-31G(d,p) basis sets for H, C, and S)<sup>11</sup> (see Supporting Information for the calculation methods and model selection) (Figures S6–S8). The adsorption Gibbs energy of **1a** was calculated at the center site of the Pd<sub>20</sub> or Au<sub>18</sub>Pd<sub>2</sub> cluster model.<sup>12</sup> The adsorption Gibbs energy of **1a** on Pd<sub>20</sub> is very high (ΔG = -48.3 kcal/mol), indicating that the metathesis product cannot easily desorb and the reaction is strongly inhibited (Figure 2b). In contrast, **1a** adsorbed on Au<sub>18</sub>Pd<sub>2</sub> has a moderate

ΔG (-24.7 kcal/mol) and the reaction can proceed (Figure 2c). The optimized structure of **1a** on Pd<sub>20</sub> clarifies strong π-adsorption between **1a** and the Pd<sub>20</sub> facets, whereas **1a** on Au<sub>18</sub>Pd<sub>2</sub> adheres via coordination of its S atom to the Pd center with almost no π-adsorption. Corroborating this finding, the natural-bond orbital charge of the phenyl group is higher in Pd<sub>20</sub>-adsorbed **1a** than in free **1a**, probably due to π-back donation from the Pd species to the phenyl rings of **1a**,<sup>13</sup> but is lower in Au<sub>18</sub>Pd<sub>2</sub>-adsorbed **1a** than in free **1a**, possibly due to σ-donation from the S atom to the Pd atom (Figure S9). Facilitated by the weak π-back donation ability of the Au species,<sup>14</sup> the Pd ensembles diluted with Au alloy changed the **1a** adsorption mode and lowered the adsorption energy to enable the reaction (Scheme 1d).<sup>15</sup> Moreover, as indicated in the optimized structure of **1a** oxidative adducts to Au<sub>18</sub>Pd<sub>2</sub>, the thiolate species produced by thioether oxidative addition on Pd species can transfer to the Au species without forming very stable structures (Figure 2d), whereas the **1a** oxidative adduct via aryl spill-over to Au species gives a slightly higher ΔG (Figure 2e).<sup>12</sup> Considering the aforementioned indirect thioether metathesis on Pd complexes,<sup>5,6</sup> thiolate spill-over onto the Au species probably promotes the transmetalation, enabling an efficient direct diaryl thioether metathesis with no additives (Scheme 1d).

In conclusion, we achieved the first heterogeneously catalyzed direct thioether metathesis using Au<sub>4.4</sub>-Pd<sub>1</sub>/TiO<sub>2</sub>. The findings in this study are anticipated to guide the development of novel molecular transformations using multimetallic catalysts, especially by harnessing metal ensembles.

## AUTHOR INFORMATION

### Corresponding Author

\*E-mail: kyama@appchem.t.u-tokyo.ac.jp, yatabe@appchem.t.u-tokyo.ac.jp

Fax: +81-3-5841-7220

### Notes

The authors declare no competing financial interests.

## ACKNOWLEDGMENT

This work was financially supported by JSPS KAKENHI Grant No. 22H04971. This work was supported by JST, PRESTO Grant Number JPMJPR227A, Japan. A part of this work was conducted at the Advanced Characterization Nanotechnology Platform of the University of Tokyo, supported by “Nanotechnology Platform” of the Ministry of Education, Culture, Sports, Science and Technology (MEXT), Japan. We thank Ms. Mari Morita (The University of Tokyo) for her assistance with the HAADF-STEM and EDS analyses. The computation was performed using Research Center for Computational Science, Okazaki, Japan (Project: 23-IMS-C002). T.M. was supported by the JSPS through the Research Fellowship for Young Scientists (Grant No. 23KJ0669).

## REFERENCES

- (1) (a) Gao, F.; Goodman, D. W. Pd–Au Bimetallic Catalysts: Understanding Alloy Effects from Planar Models and (Supported) Nanoparticles. *Chem. Soc. Rev.* **2012**, *41*, 8009–8020; (b) Li, H.; Shin, K.; Henkelman, G. Effects of Ensembles, Ligand, and Strain on Adsorbate Binding to Alloy Surfaces. *J. Chem. Phys.* **2018**, *149*, 174705; (c) Liu, P.; Nørskov, J. K. Ligand and Ensemble Effects in Adsorption on Alloy Surfaces. *Phys. Chem. Chem. Phys.* **2001**, *3*, 3814–3818.
- (2) Ishikawa, H.; Yamaguchi, S.; Nakata, A.; Nakajima, K.; Yamazoe, S.; Yamasaki, J.; Mizugaki, T.; Mitsudome, T. Phosphorus-Alloying as a Powerful Method for Designing Highly Active and Durable Metal Nanoparticle Catalysts for the Deoxygenation of Sulfoxides: Ligand and Ensemble Effects of Phosphorus. *JACS Au* **2022**, *2*, 419–427.
- (3) Greiner, M. T.; Jones, T. E.; Beeg, S.; Zwiener, L.; Scherzer, M.; Girgsdies, F.; Piccinin, S.; Armbrüster, M.; Knop-Gericke, A.; Schlögl, R. Free-Atom-Like *d* States in Single-Atom Alloy Catalysts. *Nat. Chem.* **2018**, *10*, 1008–1015.
- (4) (a) Lee, C.-F.; Liu, Y.-C.; Badsara, S. S. Transition-Metal-Catalyzed C–S Bond Coupling Reaction. *Chem. Asian J.* **2014**, *9*, 706–722; (b) Dunbar, K. L.; Scharf, D. H.; Litomska, A.; Hertweck, C. Enzymatic Carbon–Sulfur Bond Formation in Natural Product Biosynthesis. *Chem. Rev.* **2017**, *117*, 5521–5577; (c) Ihardi, E. A.; Vitaku, E.; Njardarson, J. T. Data-Mining for Sulfur and Fluorine: An Evaluation of Pharmaceuticals To Reveal Opportunities for Drug Design and Discovery. *J. Med. Chem.* **2014**, *57*, 2832–2842; (d) Lou, J.; Wang, Q.; Wu, P.; Wang, H.; Zhou, Y.-G.; Yu, Z. Transition-Metal Mediated Carbon–Sulfur Bond Activation and Transformations: An Update. *Chem. Soc. Rev.* **2020**, *49*, 4307–4359. For the reviews of synthesis of thioethers, see (e) Chauhan, P.; Mahajan, S.; Enders, D. Organocatalytic Carbon–Sulfur Bond-Forming Reactions. *Chem. Rev.* **2014**, *114*, 8807–8864; (f) Kondo, T.; Mitsudo, T. Metal-Catalyzed Carbon–Sulfur Bond Formation. *Chem. Rev.* **2000**, *100*, 3205–3220; (g) Ley, S. V.; Thomas, A. W. Modern Synthetic Methods for Copper-Mediated C(aryl)–O, C(aryl)–N, and C(aryl)–S Bond Formation. *Angew. Chem. Int. Ed.* **2003**, *42*, 5400–5449.
- (5) (a) Lian, Z.; Bhawal, B. N.; Yu, P.; Morandi, B. Palladium-Catalyzed Carbon-Sulfur or Carbon-Phosphorus Bond Metathesis by Reversible Arylation. *Science* **2017**, *356*, 1059–1063; (b) Rivero-Crespo, M. A.; Toupalas, G.; Morandi, B. Preparation of Recyclable and Versatile Porous Poly(aryl thioether)s by Reversible Pd-Catalyzed C–S/C–S Metathesis. *J. Am. Chem. Soc.* **2021**, *143*, 21331–21339.

(6) Bhawal, B. N.; Morandi, B. Catalytic Isofunctional Reactions—Expanding the Repertoire of Shuttle and Metathesis Reactions. *Angew. Chem. Int. Ed.* **2019**, *58*, 10074–10103.

(7) Matsuyama, T.; Yatabe, T.; Yabe, T.; Yamaguchi, K. Direct Thioether Metathesis Enabled by In Situ Formed Pd Nanocluster Catalysts. *Catal. Sci. Technol.* **2024**, *14*, 76–82.

(8) Previously, we reported slight thioether metathesis between **1a** and **1b** in the presence of a hydroxyapatite-supported mono-metallic Pd nanoparticle catalyst<sup>16</sup> but under very different reaction conditions, using much more catalyst (Pd: 20 mol%) at a higher reaction temperature (160°C) for 24 h.

(9) The C–S bond metathesis of **1a** and **1b** immediately ceased after hot filtration of the catalyst (Figure S3), and inductively coupled plasma–atomic emission spectroscopy (ICP-AES) detected almost zero Pd and Au species in the filtrate (Pd: below the detection limit, Au: 0.004% of the Au used in the reaction). Therefore, the observed catalysis was truly heterogeneous. After catalyst regeneration via calcination in air at 300°C followed by reduction using NaBH<sub>4</sub> in water (Figure S4), Au<sub>4.4</sub>–Pd<sub>1</sub>/TiO<sub>2</sub> obtained the same final yield of **1ab**. However, the final **1ab** yield gradually decreased after two uses of the catalyst, possibly because the Au–Pd alloy nanoparticles aggregated according to the results of STEM observations and XRD measurements (Figures S10, S11).

(10) (a) Matsuyama, T.; Yatabe, T.; Yabe, T.; Yamaguchi, K. Decarbonylation of 1,2-Diketones to Diaryl Ketones via Oxidative Addition Enabled by an Electron-Deficient Au–Pd Nanoparticle Catalyst. *ACS Catal.* **2022**, *12*, 13600–13608; (b) Yi, C.-W.; Luo, K.; Wei, T.; Goodman, D. W. The Composition and Structure of Pd–Au Surfaces. *J. Phys. Chem. B* **2005**, *109*, 18535–18540; (c) Xu, X.; Goodman, D. W. An Infrared and Kinetic Study of Carbon Monoxide Oxidation on Model Silica-Supported Palladium Catalysts from 10<sup>−9</sup> to 15 Torr. *J. Phys. Chem.* **1993**, *97*, 7711–7718; (d) Zhu, B.; Thrimurthulu, G.; Delannoy, L.; Louis, C.; Mottet, C.; Creuze, J.; Legrand, B.; Guesmi, H. Evidence of Pd Segregation and Stabilization at Edges of AuPd Nano-Clusters in the Presence of CO: A Combined DFT and DRIFTS Study. *J. Catal.* **2013**, *308*, 272–281.

(11) (a) Dhital, R. N.; Kamonsatikul, C.; Somsook, E.; Bobuatong, K.; Ehara, M.; Karanjit, S.; Sakurai, H. Low-Temperature Carbon–Chlorine Bond Activation by Bimetallic Gold/Palladium Alloy Nanoclusters: An Application to Ullmann Coupling. *J. Am. Chem. Soc.* **2012**, *134*, 20250–20253. (b) Lang, X.-F.; Yin, P.-G.; You, T.-T.; Guo, L.; Chemical Effects in SERS of Pyrazine Adsorbed on Au–Pd Bimetallic Nanoparticles: A Theoretical Investigation. *ChemPhysChem* **2012**, *13*, 237–244; (c) Miyazaki, R.; Jin, X.; Yoshii, D.; Yatabe, T.; Yabe, T.; Mizuno, N.; Yamaguchi, K.; Hasegawa, J. Mechanistic Study of C–H Bond Activation by O<sub>2</sub> on Negatively Charged Au Clusters:  $\alpha,\beta$ -Dehydrogenation of 1-Methyl-4-piperidone by Supported Au Catalysts. *Catal. Sci. Technol.* **2021**, *11*, 3333–3346; (d) Takei, D.; Yatabe, T.; Yabe, T.; Miyazaki, R.; Hasegawa, J.; Yamaguchi, K. C–H Bond Activation Mechanism by a Pd(II)–( $\mu$ -O)–Au(0) Structure Unique to Heterogeneous Catalysts. *JACS Au* **2022**, *2*, 394–406.

(12) The other adsorption sites are discussed in detail in the Supplementary Information.

(13) Wang, T.; Xu, Y.; Yang, J.; Ju, X.; Ding, W.; Zhu, Y. Predictable Catalysis of Electron-Rich Palladium Catalyst toward Aldehydes Hydrogenation. *ChemCatChem* **2019**, *11*, 3770–3775.

(14) (a) Ouyang, L.; Da, G.-J.; Tian, P.-F.; Chen, T.-Y.; Liang, G.-D.; Xu, J.; Han, Y.-F. Insight into Active Sites of Pd–Au/TiO<sub>2</sub> Catalysts in Hydrogen Peroxide Synthesis Directly from H<sub>2</sub> and O<sub>2</sub>. *J. Catal.* **2014**, *311*, 129–136; (b) Lee, J. H.; Cho, J.; Jeon, M.; Ridwan, M.; Park, H. S.; Choi, S. H.; Nam, S. W.; Han, J.; Lim, T.-H.; Ham, H. C.; Yoon, C. W. Experimental and Computational Studies of Formic Acid Dehydrogenation over PdAu: Influence of Ensemble and Ligand Effects on Catalysis. *J. Mater. Chem. A* **2016**, *4*, 14141–14147; (c) Wang, W.; Lewis, R. J.; Lu, B.; Wang, Q.; Hutchings, G. J.; Xu, J.; Deng, F. The Role of Adsorbed Species in 1-Butene Isomerization: Parahydrogen-Induced Polarization NMR of Pd–Au Catalyzed Butadiene Hydrogenation. *ACS Catal.* **2024**, *14*, 2522–2531.

(15) Previously we identified *in situ* formed Pd nanoclusters as the active species of diaryl thioether metathesis.<sup>7</sup> In that case,  $\pi$ -adsorption

of diaryl thioethers on Pd nanoclusters was probably suppressed by moderate steric hindrance of the PCy<sub>3</sub> ligand, enabling the metathesis to proceed.

(16) Matsuyama, T.; Yatabe, T.; Yamaguchi, K. Heterogeneously Catalyzed Decarbonylation of Thioesters by Supported Ni, Pd, or Rh Nanoparticle Catalysts. *Org. Biomol. Chem.* **2024**, *22*, 579–584.